Original Paper *Forma*, **16**, 141–154, 2001

Nucleation and Growth of Crystals and Formation of Cellular Pattern of Prismatic Shell Microstructure in Bivalve Molluscs

Takao UBUKATA

Institute of Geosciences, Shizuoka University, 836 Oya, Shizuoka 422-8529, Japan

(Received March 5, 2001; Accepted May 21, 2001)

Keywords: Prisms, Bivalve Shells, Theoretical Morphology, Biomineralization

Abstract. The sizes, morphologies and distribution of nucleation sites of aggregated prisms on the outer shell surface were examined in 38 species of the Bivalvia and modeled theoretically. Biometric analysis reveals the following: 1) the cellular pattern of prismatic structure tends to close with Voronoi divisions with increasing the size of prisms, and 2) nucleation of prisms tends to occur at regular intervals in the case of the low density of nucleation. Comparison of the results of biometric analysis with those of computer simulations show that the period of nucleation stage in which prisms can be born primarily controls the shapes and distribution of nucleation sites of aggregated prisms. The result of this study suggests that the crowding of nucleation is regulated so as to keep a distance between prisms.

1. Introduction

The molluscan shell consists of crystalline calcium carbonate in the form of calcite or aragonite and an organic matrix. They are arranged into various distinct fabrics, and these shell microstructures have been described by BØGGILD (1930), TAYLOR *et al*. (1969, 1973), CARTER *et al*. (1990), etc. I have been studied the geometric regularity of shell microstructures from a point of view of the pattern formation (UBUKATA, 1994, 1997a, 1997b, 2000). The shape and size of crystals reflect the physiological condition when the shell is formed (WADA, 1972, 1985). The analysis on the geometric pattern of shell microstructures, therefore, provides a reliable basis to understand the biomineralization of molluscan shells.

Among various molluscan shell microstructures, prismatic structure consists of many parallel arrayed columnar units which are called prisms (Fig. 1(b)) (CARTER and CLARK, 1985; CARTER *et al*., 1990). Each columnar unit, consisting of many smaller crystals, is surrounded and bounded by an organic matrix showing a polygonal appearance on the outer shell surface (Fig. 1(a)). Nucleation and growth of prisms occur on the substratum that is composed of a sclerotized organic film, called periostracum. The size of prisms is very variable, ranging from 3 to 60 μm in width. Recently I analyzed the size distribution of prisms in bivalves and demonstrated that the size and its variation of prisms may be a plausible index of the growth rate of the shell or prisms (UBUKATA, 2001). However, it has remained unchallenged to examine the unevenness of nucleation time within individual

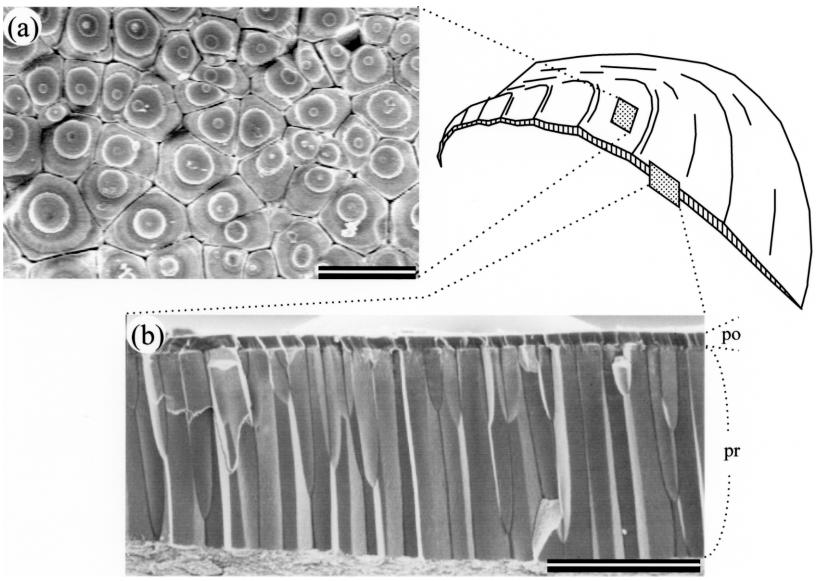

Fig. 1. Prismatic structure. SEM photographs of the outer shell surface (a) and the fractured surface (b) of the prismatic shell layer in *Anodonta woodiana* (SUM-HM-B0027), po: periostracum, pr: prismatic layer, scale: 50 μm.

prisms and the regulation of the crowding of nucleation sites, both of which may control the variation of the size of prisms.

This paper has its aim to consider the unevenness of settling time of prisms and the manner of the crowding of nucleation sites in molluscs. For this purpose, the morphologies and the distribution pattern of nucleation sites of prisms were analyzed biometrically in some species of the Bivalvia. A theoretical morphological modeling of growth kinematics of aggregated prisms was also attempted, and the results of computer simulations were compared with those of biometric analyses.

2. Material and Methods in Biometric Analyses

2.1. Preparation of specimens

A calcitic or aragonitic prismatic shell in 38 species of the Bivalvia was examined (Table 1). The species with calcitic prisms belong to Order Pterioida or Ostreoida, and those with aragonitic prisms to Unionoida or Trigonioida. Each species is represented by a single specimen. Most of them were collected at various localities around the Japanese Islands and the Philippines. All the specimens utilized are stored at Shizuoka University (SUM).

In order to remove the periostracum from the shell so as to expose the outer shell surface, the shells examined were bleached for one day. Pieces of them were washed, dried in air, coated with gold using a JEOL JFC-1500 ion coater, and observed their microstructure with a JEOL JSM-5800LV scanning electron microscope operated at 15 kV and interfaced to a computer (Dell Optiplex Gxa EM).

Table 1. List of material examined. All specimens have the prefix SUM.

Order	Species	Locality	Specimens
Pterioida	*Pteria brevialata* (Dunker)	Amakusa, Nagasaki, Western Japan	HM-B-0031
	P. penguin (Roding)	San Luice, Bathangas, Philippines	HM-B-0014
	P. sp.	Dakar, Senegal	HM-B-0032
	Pinctada martensii (Dunker)	Tateyama, Chiba, Central Japan	HM-B-0033
	P. maculata (Gould)	Iriomote Is., Okinawa, Southwest Japan	HM-B-0015
	P. margaritifera(Linnaeus)	Iriomote Is., Okinawa, Southwest Japan	HM-B-0034
	P. maxima(Jameson)	Arafura Sea	HM-B-0035
	P. nigra (Gould)	Morozaki, Aichi, Central Japan	HM-B-0036
	Isognomon perna (Linnaeus)	Iriomote Is., Okinawa, Southwest Japan	HM-B-0016
	I. ephippium (Linnaeus)	San Luice, Bathangas, Philippines	HM-B-0017
	I. legumen (Gmelin)	Iriomote Is., Okinawa, Southwest Japan	HM-B-0037
	I. nucleus Lamarck	Iriomote Is., Okinawa, Southwest Japan	HM-B-0038
	I. isognomum (Linnaeus)	San Luice, Bathangas, Philippines	HM-B-0039
	Malleus albus Lamarck	Bulan, Sorsogon, Philippines	HM-B-0040
	M. malleus (Linnaeus)	Bulan, Sorsogon, Philippines	HM-B-0041
	M. regula (Forskal)	Iriomote Is., Okinawa, Southwest Japan	HM-B-0018
	Pinna muricata Linnaeus	Honda Bay, Palawan, Philippines	HM-B-0042
	Atrina lischkeana (Clessin)	Ariake, Saga, Western Japan	HM-B-0019
	A. vexillum (Born)	Honda Bay, Palawan, Philippines	HM-B-0020
	A. teramachii Habe	Amakusa, Nagasaki, Western Japan	HM-B-0043
	A. kinoshitai Habe	Amakusa, Nagasaki, Western Japan	HM-B-0044
Ostreoida	*Crassostrea gigas* (Thunberg)	Misaki, Kanagawa, Central Japan	HM-B-0021
	C. iredalei (Faustino)	Honda Bay, Palawan, Philippines	HM-B-0045
	Saccostrea mordax (Gould)	Iriomote Is., Okinawa, Southwest Japan	HM-B-0046
	S. echinata (Quoy & Gaimard)	Iriomote Is., Okinawa, Southwest Japan	HM-B-0047
	S. sp.	Iriomote Is., Okinawa, Southwest Japan	HM-B-0048
	Ostrea denselamellosa Lischke	Sagami Bay, Kanagawa, Central Japan	HM-B-0049
	Neopycnodonte cochlear (Poli)	Misaki, Kanagawa, Central Japan	HM-B-0050
	Hyotissa inaequivalvis (Sowerby)	Iriomote Is., Okinawa, Southwest Japan	HM-B-0051
Unionoida	*Margaritifera laevis* (Haas)	Nakagawa, Hokkaido, Northern Japan	HM-B-0022
	Inversidens reiniana (Kobelt)	Lake Biwa, Shiga, Central Japan	HM-B-0023
	Unio biwae Kobelt	Lake Biwa, Shiga, Central Japan	HM-B-0024
	Lanceolaria oxyrhyncha (Martens)	Lake Biwa, Shiga, Central Japan	HM-B-0025
	Lamprotula rochechoarti (Heude)	Tung-t'ing Lake, China	HM-B-0052
	Anodonta woodiana (Lea)	Lake Biwa, Shiga, Central Japan	HM-B-0026
	A. calypygos Kobelt	Lake Biwa, Shiga, Central Japan	HM-B-0028
	Cristaria plicata (Leach)	Lake Biwa, Shiga, Central Japan	HM-B-0029
Trigonioida	*Neotrigonia margaritacea* (Lamarck)	French Is., Australia	HM-B-0030

2.2. Measuring the size of prisms

Areas of prisms on the outer shell surface were measured at the 2–7 portions along a growth ring on the shell surface of each specimen. For details of the technique to measure the sizes of prisms, refer to UBUKATA (2001). An SEM image of the measured portion was saved as a computer bitmap file. Next, the boundaries between adjoining prisms of the

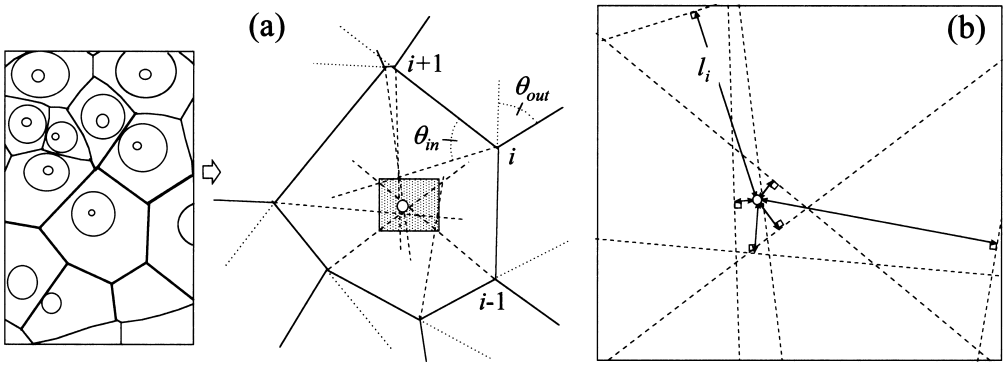

Fig. 2. Determining the center of an approximated Voronoi polygon. An additional line from the vertex *i* to the inside of the polygon (dashed lines) is drawn where $\theta_{in} = \theta_{out}$. The approximated center is determined so as to minimize the sum of squares of l_i. (b): An enlargement of the dotted area of (a).

image were traced on a personal computer, and then each prism was filled with a different color. Subsequently, the area of each prism was measured by counting the pixels with the same color. For measuring the areas of prisms, a computer program written in *Visual Basic* Version 6.0 was used on a personal computer.

Since the size-frequency distribution of the areas of prisms is generally right-skewed (UBUKATA, 2001), the mean is not suitable for representing the "average" size of prisms. In this study, an "average" area of prisms on a shell portion was represented by the median of the areas ($\tilde{S}$).

2.3. Shape of polygons of prisms

UBUKATA (1994) reported that many small hemispherical incipient prisms occur at the growing shell margin. Many growth rings are often observed within an individual prism since growth of a prism is represented by an enlarging circle (Fig. 1(a)). As the prisms grow, neighboring prisms come in contact with one another, as a result of formation of a boundary between two prisms. If prisms start to grow simultaneously, each prism is expressed as a Voronoi polygon, a polygon whose interior domain consists of all points which are closer to the center of the domain than to any other centers of domains. Then, how far the pattern of prisms deviates from that of Voronoi divisions is expected to represent the unevenness of nucleation time among prisms. In the present paper, the deviation from Voronoi polygons was represented by Δ value of HONDA (1978, 1983).

A domain of an actual prism, which does not correspond to an exact Voronoi polygon, can be regarded as an approximated Voronoi polygon. According to HONDA (1983), the center of an approximated Voronoi polygon was determined as follows. At the first step, an additional line from the vertex *i* to the inside of the polygon is drawn where $\theta_{in} = \theta_{out}$ (Fig. 2(a)). In the case of an exact Voronoi polygon, additional lines from all vertices (dashed lines in Fig. 2(a)) intersect in a point which is the center of the Voronoi polygon. In the case of an actual prismatic domain, the approximated center is determined so as to

minimize the sum of squares of the distance from the center to each additional line. The deviation of a polygon *j* from the Voronoi division is defined as:

$$\Delta_j = \left(\sum_{i=1}^{n_j} l_i^2 \right)_{\min} \Big/ n_j ,$$

where l_i is the distance from the center to the additional line drawn from the vertex *i* (Fig. 2(b)), and n_j is the number of vertices of the *j*-th polygon. Δ_j, the area of the *j*-th polygon (S_j), and the number of polygons (N) define the Δ value:

$$\Delta = \left(\sum_{i=1}^{N} \Delta_j \right) \Big/ \left(\sum_{i=1}^{N} S_j \right).$$

Δ is zero in the case of exact Voronoi polygons, and the value becomes small as the pattern resembles Voronoi divisions. The value of Δ was estimated in every shell portion examined.

2.4. Spatial distribution pattern of nucleation sites

The spatial distribution pattern of nucleation sites of prisms was analyzed by use of the value of the "mean crowding" (LLOYD, 1967), as described below. An SEM image was divided into squared grids of an arbitrary size and the number of nucleation sites of prisms was counted in each square (Fig. 3(a)). The number of squares and nucleation sites in each square both define the mean crowding of LLOYD (1967), which represents the mean number of other individuals in the same square for an individual. The mean crowding is defined as:

$$\overset{*}{x} = \sum_{i=1}^{n} x_i (x_i - 1) \Big/ \sum_{i=1}^{n} x_i ,$$

where n is the number of squares and x_i is the number of sites in the square *i*.

The value of $\overset{*}{x}$ depends on the mean number of individuals per square (mean density; $\bar{x}$), and a linear correlation is expected to be found between $\overset{*}{x}$ and $\bar{x}$ (Fig. 3(b)) (IWAO, 1968). IWAO (1968) proposed the use of the regression of the mean crowding on the mean density for analyzing the aggregation pattern of an animal population. The $\overset{*}{x}$-intercept of the regression line, which is called the index of basic contagion (α), represents the degree of aggregation of individuals. α is expected to be positive when individuals tend to gather, whereas it is expected to be negative when individuals keep away from one another. Thus, α decreases as the distribution becomes uniform. When the spatial distribution pattern of individuals is exactly uniform, $\alpha = -1$. In the present study, the value of α was estimated in every shell portion examined.

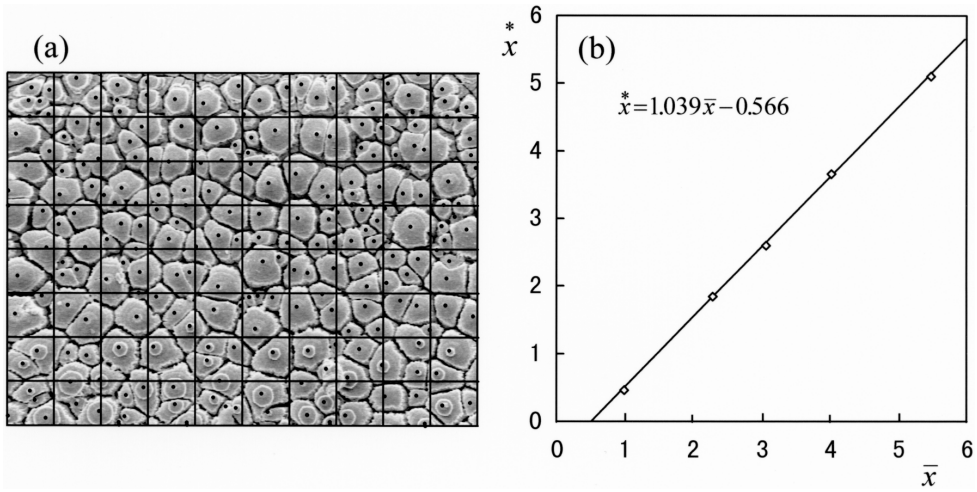

Fig. 3. Determining the index of basic contagion (α). An SEM image was subdivided into a squared grid, and the number of nucleation sites of prisms (bold points) was counted in each square (a). If the mean number per individual of other individuals in the same square is expressed by $\overset{*}{x}$, the $\overset{*}{x}$-intercept of the regression line of $\overset{*}{x}$ on the mean density $\bar{x}$ defines α (b).

3. Modeling of Prism Growth

For better understanding the relationships between the average size of prisms and the unevenness of nucleation time and/or the distribution pattern of nucleation sites of prisms, the growth of aggregated prisms was modeled theoretically. Recently I introduced a growing circles model to represent growth of prisms (UBUKATA, 2001). In this model, growth of a prism is represented by kinematics of an enlarging circle. In the present study, a modified version of the growing circles model was used to illustrate theoretical morphology of prismatic structure.

WEINER and TRAUB (1984) proposed an interesting model of biomineralization of molluscan shell that the nucleation site within the shell is composed of acidic proteins distributed in a localized area on the matrix protein and constitutes only a small part of the total matrix protein. In the present model, the potential nucleation sites of prisms are assumed to be distributed discretely and are placed at lattice points which are regularly arranged. The distance between the neighboring potential nucleation sites is expressed by d, which represents the unit size (Fig. 4(a)). Each prism is approximated by a circle which enlarges at a steady rate. Over a single short period, calcium carbonate is precipitated along the circumference of each prism giving rise to the shaded portion in Fig. 4(a), and the radius of each circle increases by ΔR. As the prisms grow, neighboring prisms come in contact with one another, as a result of formation of a boundary between two prisms (Fig. 4(c)). A unit interval of growth step is defined as the period during which the radius of each circular prism increases by d. Then, Δs steps are generally defined as:

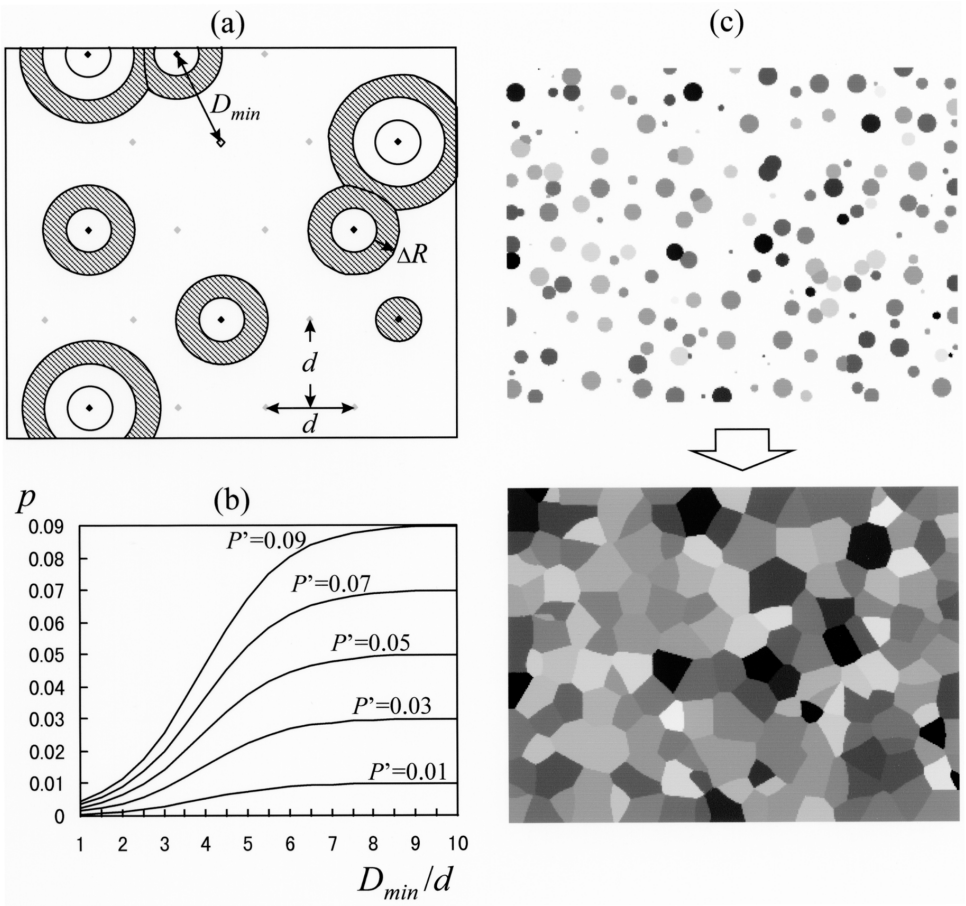

Fig. 4. The growing circles model. Black bold points in (a) indicate initiation sites of produced prisms, and gray ones potential nucleation sites of unborn prisms. In the case of regulating the crowding of nucleation, the probability of nucleation in a potential site decreases logistically and approaches to P' (b). As the prisms grow, neighboring prisms come in contact with one another, as a result forming a boundary between two prisms (c).

$$\Delta s \equiv \Delta R / d.$$

It is assumed that prisms can be born within a given period of early growth stage of aggregated prisms, as a result of irregularity of the settling time among prisms (UBUKATA, 1994). The period of the nucleation stage, which means the unevenness of nucleation time among prisms, is represented by V steps. A growing circle often occupies the space in which a neighboring "unborn" prism starts to grow. In computer simulations, crowding of newborn prisms was assumed to be regulated or not. If we accept the latter assumption, nucleation of prisms occurs randomly at a potential nucleation site during each growth step

of the nucleation stage with a probability of *P*. Under the assumption of the former case, the probability of nucleation at a potential site increases logistically as the distance between the site and its neighboring prism increases (Fig. 4(b)). In this case, the probability of nucleation per unit growth step at the site *i* is defined as:

$$p = P' / \left(1 + 1000 \exp\left(-0.5 D_{\min} / d\right)\right),$$

where $D_{\min}$ is the distance between the site *i* and the center of the nearest existing prism to *i* (Fig. 4(a)), and P' is an asymptotic value of the probability of nucleation per unit growth step (Fig. 4(b)).

Now, we can perform a computer simulation for growth of hypothetical prisms if two parameters *V* and *P* or P' are given. Subsequently, the area of a hypothetical prism was measured as the number of pixels on the display surface, and the median of the area of hypothetical prisms ($\tilde{S}_{st}$) was estimated in each model. The coordinates of a nucleation site were recorded on each hypothetical prism for calculating α in a model. The value of Δ was also estimated in each model. Computer simulations were carried out with a program written in *Visual Basic* Version 6.0 by means of a 64 bit workstation computer (Visual Technology VT-Alpha 600) interfaced with a CRT (Iiyama A702H).

4. Results

4.1. Biometric analyses

As a result of the biometric analyses, a negative correlation or an inverse relationship was found between Δ and $\tilde{S}$ both in species with calcitic and aragonitic prisms (Fig. 5(a)).

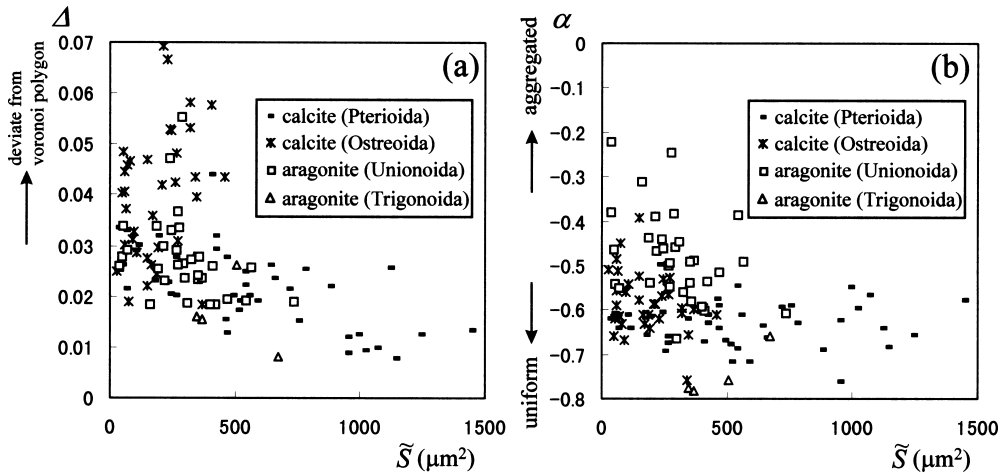

Fig. 5. Relationships between $\tilde{S}$ and Δ (a), and between $\tilde{S}$ and α (b) in actual shells.

The inverse relationship between Δ and $\tilde{S}$ is clear especially in species with calcitic prisms, while it seems to be more or less obscure in species with aragonitic prisms. The result shows that the cellular pattern of prismatic structure tends to close with Voronoi polygons with increasing the average size of prisms, particularly in species with calcitic prisms.

In all specimens examined, $\alpha < 0$, which indicates that nucleation sites of prisms tend to be distributed uniformly (Fig. 5(b)). This fact suggests that a newborn prism tends to occur so as to keep a distance from other existing prisms. α appears to be negatively correlated with $\tilde{S}$ at the level of 1% significance in species with aragonitic prisms (Fig. 5(b)). In the case of calcitic prisms, α is inversely related to $\tilde{S}$, though the relationship is graphically unclear particularly in the high $\tilde{S}$ region (Fig. 5(b)). The range of α in aragonitic prisms is broader than that in calcitic prisms. The negative or inverse relationship between α and $\tilde{S}$ indicates that nucleation of prisms tends to occur at regular intervals in the case of the low density of nucleation.

4.2. Computer simulations

$\tilde{S}_{st}$, which means an "average" size of hypothetical prisms, tends to be inversely proportional to both *V* and *P*, whether the crowding of newborn prisms is regulated (Fig. 6(b)) or not (Fig. 6(a)). This is because the frequency of nucleation increases as the period of the nucleation stage or the probability of nucleation either increases.

Δ, which represents the deviation from Voronoi polygons, is positively correlated with *V*, whether the crowding of newborn prisms is regulated (Fig. 6(d)) or not (Fig. 6(c)). As a result, comparison of Δ with $\tilde{S}_{st}$ arrives at an inverse relationship between them in each case (Figs. 7(a) and (b)). This relationship is concordant with that from biometric analyses (Fig. 5(a)). Since *V* defines the period of the nucleation stage, these results indicate that the deviation from Voronoi polygons represents well the unevenness of nucleation time among prisms.

α, which indicates the degree of the aggregation of nucleation sites, is negatively correlated with *V* on the assumption of random nucleation (Fig. 6(e)), while it tends to increase with increasing *V* when the crowding of nucleation is regulated (Fig. 6(f)). In consequence, α tends to increase with increasing $\tilde{S}_{st}$ when nucleation occurs randomly at a potential site (Fig. 7(c)), since small prisms tend to gather around a large prisms under this condition. On the other hand, α is negatively correlated with $\tilde{S}_{st}$ when the crowding of nucleation is regulated (Fig. 7(d)). The correlation of the latter case is concordant with that from biometric analyses (Fig. 5(b)). This fact supports the assumption that the crowding of nucleation is regulated so as to keep a distance between prisms.

5. Discussion

To sum up the biometric analyses and computer simulations, the period of the nucleation stage in which prisms can be born is considered to be the primary control determining the shapes and distribution of prisms (Fig. 8). If the stage of nucleation of prisms extends over a long period, a plenty of incipient prisms tend to be distributed ununiformly at a high density, and the cellular pattern of prismatic structure deviates far

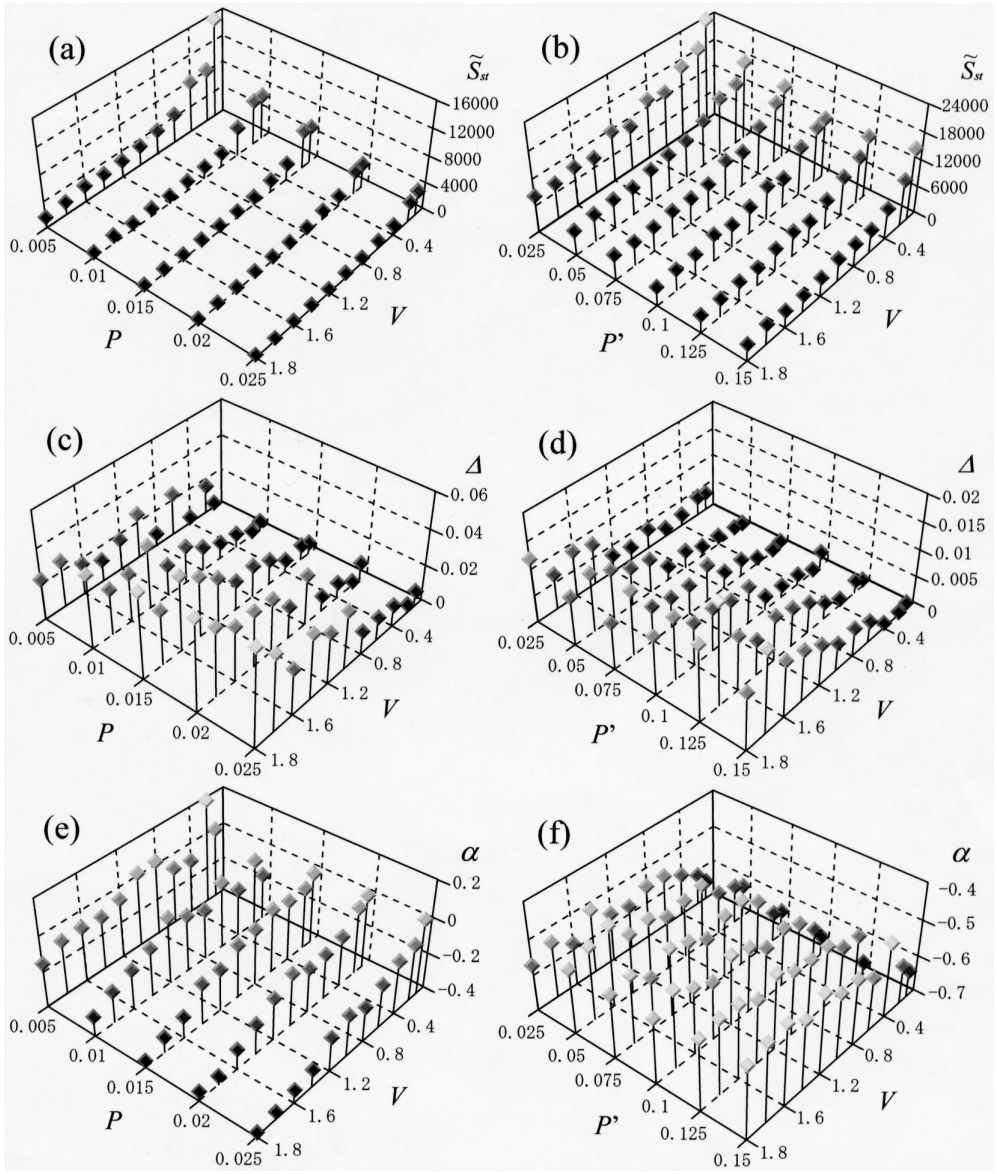

Fig. 6. Three dimensional scatter diagrams illustrating the values of $\tilde{S}_{st}$, α or Δ of hypothetical prisms in relation to V and P or P'. The crowding of nucleation is regulated ((b), (d), (f)) or not ((a), (c), (e)).

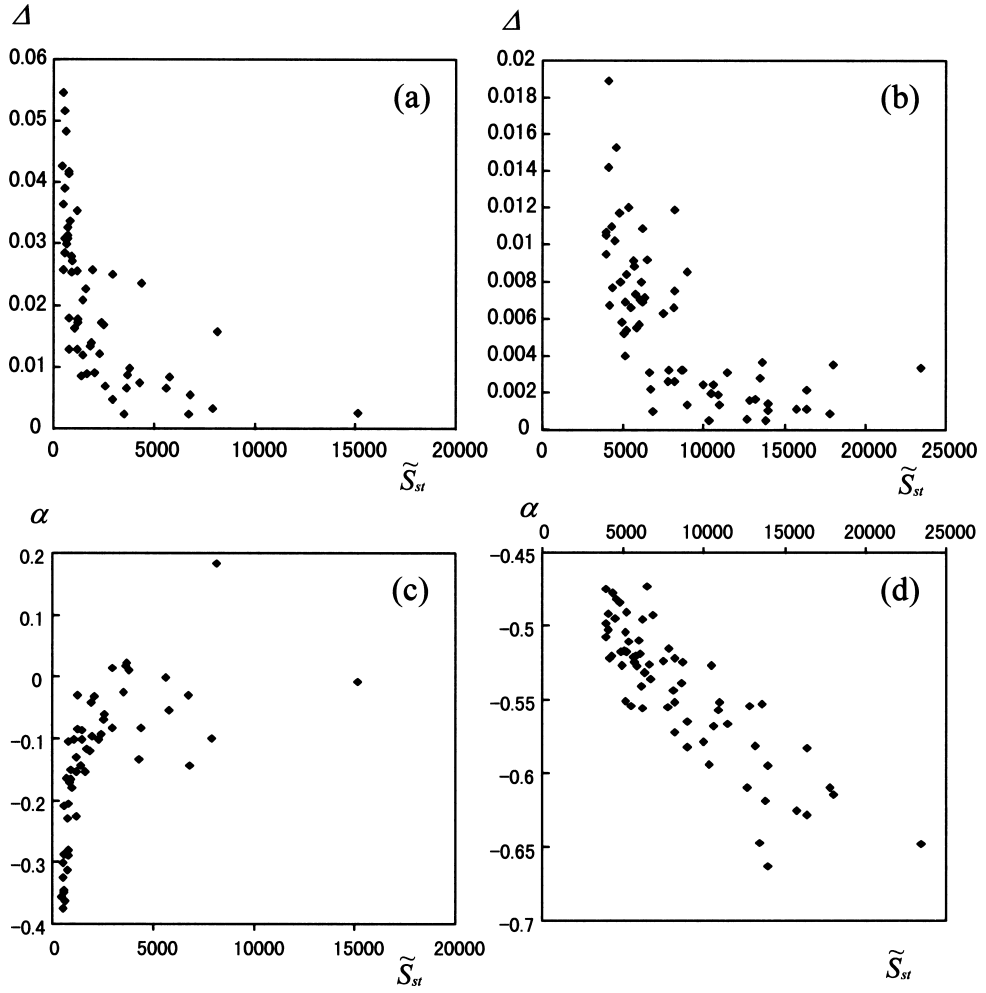

Fig. 7. Relationships between $\tilde{S}_{st}$ and Δ, and between $\tilde{S}_{st}$ and α in theoretical models. Nucleation occurs randomly at a potential site ((a), (c)) or the crowding of nucleation is regulated ((b), (d)).

from Voronoi polygons (Fig. 8(d)). The period of the nucleation stage extends with widening the nucleation zone on a inner surface of the periostracum and/or with decreasing the growth rate of the shell. UBUKATA (2001) showed that the size and its variation of prisms both correlate with the growth rate of the shell, and that the size of prisms increases and its variation decreases as the shell grows faster. The present study suggests that the morphologies and the distribution of nucleation sites of prisms are also specious indices of the shell growth rate.

UBUKATA (1994, 1997a) claimed that relatively slow growth of the shell produces prisms prominently inclined to the outer shell surface, because of the retarding the

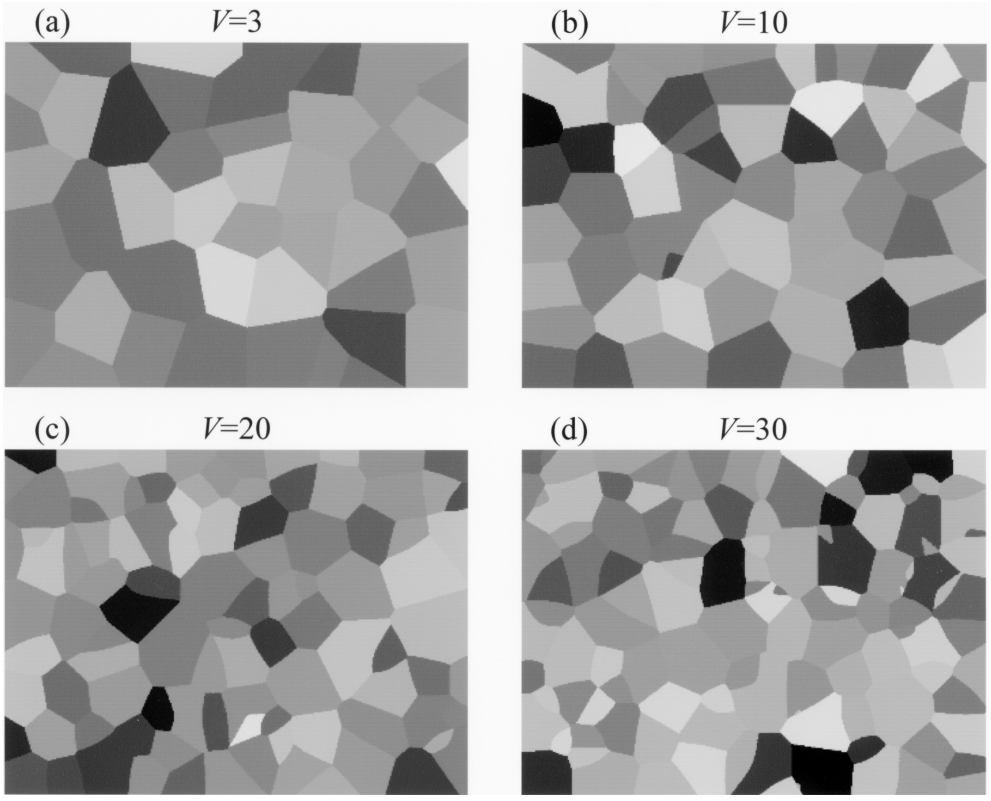

Fig. 8. Display of the growing circles model when the crowding of nucleation is regulated and $P' = 0.15$. Each prism is identified by several shades of gray. As V increases, the average size of prisms decreases, distribution of nucleation sites becomes more ununiform, and the shape of prisms diverges away from that of Voronoi polygons.

initiation of their forward growth relative to the radial direction. Such an inclined prisms is commonly found in the species belonging to the Unionidae and Ostreidae (UBUKATA, 1994), and their prisms also characteristically occur in a low $\tilde{S}$ (small size) and high Δ (deviating from Voronoi polygons) or high α (ununiform distribution of nucleation sites) region in Fig. 5. As mentioned above, the present study suggests that characteristic pattern of prisms as seen in the Unionidae and Ostreidae is produced under the condition of slow growth of the shell. The result of the present study is consistent with that of UBUKATA (1994, 1997a).

This study indicates that the crowding of nucleation of prisms is regulated so as to keep a distance between prisms, although the mechanism is unknown. Compared with other shell microstructures, prismatic structure consists of especially large structural units. Another characteristic feature of the prismatic structure is variable sizes of its structural units which is recognized even within a single shell. In order to form a large prism, generation of many

small seeds of crystals around the prism should be avoided since such seeds inhibit growth of the prism. If an extremely low density of potential nucleation sites is adopted, a new born seed can grow to a large prism, but relatively small prisms can not be formed. Therefore, high density of potential nucleation sites and regulation of the crowding of produced prisms may make possible forming quite variable sizes of prisms in bivalve shells.

The process of formation of the shell microstructure is closely related to crystallographic and biochemical aspects of biomineralization which are controlled ultimately by the genetic program. However, clarifying the architectural process of the structure also needs recognition of the algorithm of morphogenesis or pattern formation. Analyzing the geometric pattern of aggregated biominerals on the basis of theoretical morphology is useful for understanding the process itself. For linking the geometric pattern with biomineralogical nature, more elaborate methods in which crystallographic and biochemical aspects are incorporated should be required.

I thank Professor K. Tanabe (University of Tokyo) and anonymous referees for critical review of manuscript. This study has been supported by Grant-in-Aid for Scientific Research (A) from the Japan Society for the Promotion of Science (No. 10304040).

REFERENCES

BØGGILD, O. B. (1930) The shell structure of the Mollusks, *Det Kongelige Danske Videnskabernes Selskabs Skrifter, Naturvidenskabelig og Mathematisk, Afdeling, Ser. 9*, **2**, 231–326.

CARTER, J. G. and CLARK, G. R., II (1985) Classification and phylogenetic significance of molluscan shell microstructure, in *Mollusks: Notes for a Short Course* (ed. T. W. Broadhead), pp. 50–71, University of Tennessee, Knoxville.

CARTER, J. G., BANDEL, K., DE BUFFRÉNIL, V., CARLSON, S. J., CASTANET, J., CRENSHAW, M. A., DALINGWATER, J. E., FRANCILLON-VIEILLOT, H., GÉRAUDIE, J., MEUNIER, F. J., MUTVEI, H., DE RICQLÈS, A., SIRE, J. Y., SMITH, A. B., WENDT, J., WILLIAMS, A. and ZYLBERBERG, L. (1990) Glossary of skeletal biomineralization, in *Skeletal Biomineralization: Patterns, Processes and Evolutionary Trends*, Vol. 1 (ed. J. G. Carter), pp. 609–671, Van Nostrand, New York.

HONDA, H. (1978) Description of cellular patterns by dirichlet domains: the two dimensional case, *J. Theor. Biol.*, **72**, 523–543.

HONDA, H. (1983) Geometrical analysis of cells becoming organized into a tensile sheet, the blastular wall, in the starfish, *Differentiation*, **25**, 16–22.

IWAO, S. (1968) A new regression method for analyzing the aggregation pattern of animal populations, *Res. Popul. Ecol.*, **10**, 1–20.

LLOYD, M. (1967) 'Mean crowding', *J. Anim. Ecol.*, **36**, 1–30.

TAYLOR, J. D., KENNEDY, W. J. and HALL, A. (1969) The shell structure and mineralogy of the Bivalvia. Introduction, Nuculacea-Trigonacea, *Bull. Br. Mus. Nat. Hist. (Zool.)*, **3**, Suppl., 1–125.

TAYLOR, J. D., KENNEDY, W. J. and HALL, A. (1973) The shell structure and mineralogy of the Bivalvia. II. Lucinacea-Clavagellacea. Conclusions, *Bull. Br. Mus. Nat. Hist. (Zool.)*, **22**, 253–294.

UBUKATA, T. (1994) Architectural constraints on the morphogenesis of prismatic structure in Bivalvia, *Palaeontology*, **37**, 241–261.

UBUKATA, T. (1997a) Microscopic growth of bivalve shells and its computer simulation, *The Veliger*, **40**, 165–177.

UBUKATA, T. (1997b) Mantle kinematics and formation of commarginal shell sculpture in Bivalvia, *Paleont. Res.*, **1**, 132–143.

UBUKATA, T. (2000) Theoretical morphology of composite prismatic, fibrous prismatic and foliated shell microstructures in bivalves, *Venus*, **59**, 297–305.

UBUKATA, T. (2001) Geometric pattern and growth rate of prismatic shell structures in Bivalvia, *Paleont. Res.*, **5**, 33–44.

WADA, K. (1972) Nucleation and growth of aragonite crystals in the nacre of bivalve molluscs, *Biomineralization*, **6**, 141–159.

WADA, K. (1985) Growth of $CaCO_3$ crystals in bivalve shell mineralization, *J. Japan. Ass. Cryst. Growth*, **12**, 57–70 (in Japanese with English abstract).

WEINER, S. and TRAUB, W. (1984) Macromolecules in mollusc shells and their functions in biomineralization, *Phil. Trans. R. Soc. Lond. B*, **304**, 425–434.